Radar-based measurement of solids back-mixing in the freeboard of a circulating fluidized bed

Chemical Engineering Journal 488 (2024) 151150

Contents lists available at ScienceDirect

Chemical Engineering Journal

journal homepage: www.elsevier.com/locate/cej

Radar-based measurement of solids back-mixing in the freeboard of a circulating fluidized bed

Wanqiang Wu [a,b], Diana Carolina Guío-Pérez [b], Marlene Bonmann [c], Filip Johnsson [b], Lunbo Duan [a], David Pallarès [b,*]

[a] Key Laboratory of Energy Thermal Conversion and Control, Ministry of Education, School of Energy and Environment, Southeast University, 210096 Nanjing, China
[b] Department of Space, Earth and Environment, Division of Energy Technology, Chalmers University of Technology, 41296 Gothenburg, Sweden
[c] Department of Microtechnology and Nanoscience, Terahertz and Millimetre Wave Laboratory, Chalmers University of Technology, 41296 Gothenburg, Sweden

ARTICLE INFO

Keywords:
Circulating fluidized bed
Solids mixing
Solids disengagement
Sub-millimeter wave radar diagnostics
Doppler effect

ABSTRACT

This work investigates solids back-mixing in the freeboard of a circulating fluidized bed based on THz-radar measurements of the concentrations and velocity distributions of the solid particles along the height of the riser. These data allow height-resolved closure of the solids mass balance and, thereby, quantification and further insight of the two main mechanisms for the back-mixing of the solids entrained from the bottom region of the fluidized bed: (i) solids disengagement and backmixing within the core region of the riser cross-section,; and (ii) solids lateral transfer of from the core region to the wall layers. The experiments were carried out in a circulating fluidized bed riser (3.1 m in height and 0.45 m^2 in cross-section), which was operated with Geldart B solids fluidized with air at room temperature and for different gas velocities. The experimentally-derived data are expressed in terms of the disengagement rate and a lateral core-to-wall layer mass transfer coefficient. From the results, it is estimated that the presence of disengagement-based solids back-mixing is significant all along the 3-m riser. The disengagement rate shows a non-linear dependency on the solids concentration, with the lateral solids transfer to the walls (which follows a linear dependency on the solids concentration) eventually becoming the dominant form of back-mixing at upper heights.

1. Introduction

Circulating fluidized bed (CFB) technology is a mature reactor type that is employed in different industrial sectors. A major application of the CFB technology has been for heat and power production in boilers, for which industrial-scale units have been available commercially for more than three decades. This application of CFBs has as its main advantages inherent emissions control (of NO_x and SO_x) and fuel flexibility [1,2]. In addition, energy transition and decarbonization is pushing the development of CFB-based applications beyond combustion, such as biomass pyrolysis or gasification [3], CO_2 capture [4], or thermochemical energy storage [5]. All these CFB applications use Geldart B solids (ash remaining from the solid fuel, makeup sand, limestone particles) as the bed material, yielding qualitatively different with those of CFB units operated with Geldart A solids (e.g., fluid catalytic crackers; FCC) [5,6]. With the solids flow being crucial to the closure of the mass and heat balances used in the design, operation, and scale-up of CFB units [7], extensive theoretical and experimental studies have been carried out to characterize the key parameters of the solids flow, such as solids concentration, velocity, residence time and cluster formation [8–11]. However, an in-depth understanding of the solids flow is still lacking, due to both the high computational costs of fine-grained gas-solids CFD modeling and the difficulties associated with collecting experimental data with high enough accuracy and resolution.

At present, several measurement techniques are used to study the solids flow in fluidized beds. Pressure drop measurements [12–15] are widely used to calculate the vertical profile of the average solids concentrations in industrial installations, and are also commonly used in research units. While the pressure measurement method is simple, cheap and robust in terms of the hardware used, it has the following drawbacks: (i) it is not straightforward to interpret for which spatial region the obtained solids concentration values are representative; (ii) solids acceleration influences the measured pressure values, thereby distorting the calculated solids concentration values [16]; (iii) the spatial resolution is often limited by the extended distance between the pressure taps [17] (and thus, indirectly by the sensitivity of the pressure transducer); and (iv) the measurement becomes inaccurate at very low

* Corresponding author.
E-mail address: david.pallares@chalmers.se (D. Pallarès).

https://doi.org/10.1016/j.cej.2024.151150
Received 22 December 2023; Received in revised form 1 April 2024; Accepted 8 April 2024
Available online 9 April 2024

Nomenclature

A	Area, m2
c_0	Speed of light, m/s
C	Concentration, kg/m^3
f_c	Center frequency, Hz
f_d	Doppler shift, Hz
f_{ext}	Scaling factor of σ_e
f_{PSD}	Particle size distribution probability function
F	Solid mass flow, kg/s
g	Gravitational acceleration, m/s^2
G	Solids flux, kg/m^2·s
h	Height, m
H_b	Dense bed height, m
h_m	Horizontal core-to-wall layer mass transfer coefficient, m/s
K	Decay constant in transport zone, m-1
n	Number concentration, part/m^3
r	Radius of a single particle, m
r_{diseng}	Net disengagement volumetric rate, kg/m^3·s
R	Radar range, m
P_r	Reflected signal power, W
u	Velocity, m/s
V	Volume, m^3
x, y, z	Coordinate system orientation

Greek letters

α	Coefficient for net volumetric clustering rate, kg/m^3·s
β	Probability density function
ε	Volumetric concentration, m^3/m^3
ρ	Solid density, kg/m^3
$\rho_{s,entr}$	Concentration of the solids entrained from the bottom region, kg/m^3
$\rho_{s,Hb}$	Concentration of the solids in the dense phase, kg/m^3
σ_b	Single-target backscattering cross section, m^2
σ_e	Effective extinction cross section, m^2

Subscripts

bot	Bottom region
core	Core region
down	Downflowing
g	Gas
lat	Lateral
s	Solid
top	Top region
up	Upflowing

Abbreviations

CFB	Circulating fluidized bed
CFD	Computational fluid dynamics
FCC	Fluid catalytic crackers
FMCW	Frequency-Modulated Continuous Wave
HDPE	High-density polyethylene

concentrations. More-advanced measurement methods are being developed that aim at higher levels of spatial resolution and accuracy, e.g., using optical probes [18–20], high-speed cameras [21-23], x/γ-ray systems [24,25], and electrical capacitance systems [26,27]. However, the implementation of these techniques in larger units is challenging with respect to achieving adequate penetration lengths and sufficiently high levels of spatial resolution. The solids back-mixing has been studied experimentally in industrial units by means of optical probes [28,29] and in laboratory-scale narrow units by means of advanced diagnostics, e.g., radioactive solids tracking [30]. However, there is in literature a lack of high-resolution measurement data for the back-mixing of Geldart B solids in CFB units under conditions relevant to industrial operation. Such units are typically characterized by a low height-to-width aspect ratio for both the riser (<10) and the bottom bed (<1); and a net circulating solids flux < 20 kg/m^2·s [6].

The use of radar technology for experimental investigations of solids flows has advantages: non-invasiveness; extended penetration lengths; and high spatial and temporal resolutions [31]. The radar technology offers the possibility to measure remotely the velocity distribution and the concentration of the particulate phase within a large volume [32–34]. The pneumatic transport of Geldart C particles (e.g. in food industry) or fast fluidization of A particles (e.g. in fluid catalytic cracking) exhibits little back-mixing yielding to the concept of saturation carrying capacity. As discussed in detail in [35], this is in contrast with the solids flow pattern established in the main industrial application of fluidization for B particles (fluidized bed combustors or gasifiers), where under circulating conditions a significant solids back-mixing is exhibited all along the furnace height [36]. Baer et al. [37] demonstrated the high accuracy attained using Frequency-Modulated Continuous Wave (FMCW) radar systems in measuring by integral means (i.e. not spatially- resolved) the cross-sectional average solids concentration in a pneumatic conveying riser with Geldart C and A particles (. By studying the time shift between the time series of averaged solids concentration at two different riser heights, they derived an average solids velocity. Recent development of the FMCW-pulse Doppler radar has enabled accurate measurements of solids concentration [31] and particle velocity distributions [38], including solids flows with higher solids concentrations (with solids volumetric concentrations up to the order of 0.1) [31], with sub-millimeter spatial resolution.

This work aims to investigate, through quantitative evaluation, the solids back-mixing in the freeboard of a circulating fluidized bed using Geldart B solids. For this, an experimental investigation was carried out that provides height-resolved closure of the solids mass balance and thus, the values of the parameters governing the solids back-mixing (i.e., the disengagement rate and the core-to-wall layer transfer coefficient). The measurements of the velocity distributions and concentration of the solids phase along the riser height were performed using FMCW-pulse Doppler radar. The main novelty of this work lies in the spatially-resolved analysis of the solids flow, thanks to the simultaneous and spatially-resolved measurement of both solids concentration and velocity distribution.

The scope of this work is limited to solids flow conditions relevant to large-scale CFB risers such as those currently used in CFB boilers, i.e., risers that use Geldart group B solids and have a riser cross-section that is sufficiently wide to provide a solids flux that is flat over the core with downward-flowing solids wall layers.

2. Theory

2.1. Solids back-mixing: Vertical disengagement and horizontal mass transfer

The macroscopic solids flow pattern in the freeboard of a CFB riser that is operated with Geldart B solids adopts a core-annulus pattern. In the core region, a net upflow of solids is established that consists of a mix of: (i) solids flowing downwards, e.g. larger particles (in upper, more dilute regions) or solids strand formations (in lower, denser regions such as the splash zone [39]) that are back-mixed downwards in the core region due to e.g. size- or density-driven solids disengagement; and (ii) solids flowing upwards, dragged by the gas flow while dispersing

horizontally and thus possibly being at some point transferred to the annulus region, consisting of downflowing wall-layers which back-mix such transferred solids externally to the core region. Measurements in industrial-scale CFB boilers show that the downwards solids phase is almost completely absent in the upper regions of such riser furnaces (typically having heights in the tens of meters) [8]. Further measurements indicate that there is a net transfer of solids from the core region to the riser walls, creating downward-flowing layers of solids with increasing solids concentration and thickness as one moves down along the riser walls [40]; through this mechanism, solids are recirculated back into the bottom bed [8,41,42]. This internal solids circulation caused by the back-mixing to the wall layers is for CFB boilers much greater than the external circulation of solids that takes place through the primary cyclone and loop seal [43].

To quantify this internal circulation, a differential mass balance of the solids can be formulated over a horizontal slice of the core region in the freeboard, as shown in Fig. 1 and described previously [42]. In this mass balance, there is a solids upflow and a solids downflow with transfer of the solids population in the two directions between these two phases, i.e., downflowing solids can be re-entrained by the upflowing gas. At the same time, the trajectories of some of the upflowing solids will cause them to end up in the wall layers at a rate that reflects the net transfer from the upwards solids phase to the wall-layer solids phase, i.e., the solids back-mixing by horizontal mass transfer. With the existing limitations in relation to experimental diagnostics, the phenomenon of solids disengagement has been mostly studied through modeling (see for example [44]). However, as this is a key event in the gas-solids momentum transfer, it needs to be fully understood (e.g., through sub-grid models). As for the solids back-mixing via lateral mass transfer to the wall layers (F_{lat} in Fig. 1), it has been suggested that this is governed by a turbophoresis process (see for example [41]).

The rather flat horizontal solids flow profiles in the core region of wide CFB risers differ from the parabolic shapes that are characteristic of narrow risers [43,45]. This flat profile of solids flux across the core region has been verified for the setup used in this work, through previous radar measurements acquired using a horizontally oriented beam [46]. Therefore, it can be said that, at a given height, the local solids concentration and vertical velocity distribution are representative of the whole core region.

According to the mass balance in Fig. 1, the net volumetric disengagement rate is the solids downflow mass change per unit volume, which can be calculated through the mass balance for the downflowing solids phase:

$$r_{\text{diseng}} V = F_{\text{down,bot}} - F_{\text{down,top}} = \left(G_{\text{down,bot}} - G_{\text{down,top}}\right) A_{\text{z,core}} \tag{1}$$

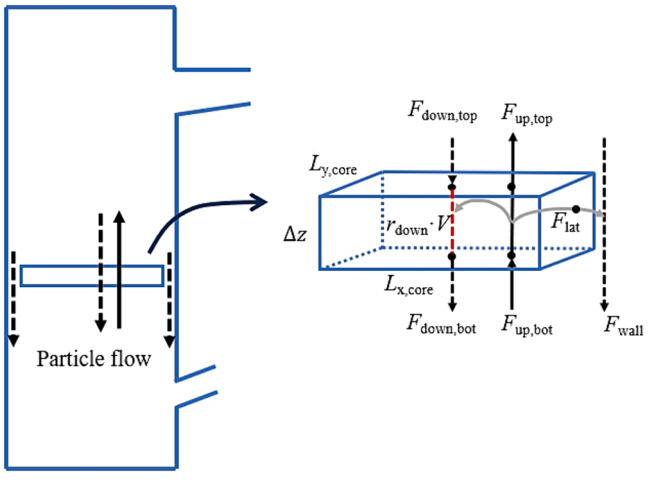

Fig. 1. The solids mass balance over a horizontal slice in the core region of the CFB freeboard.

Assuming that the horizontal cross-sectional area of the wall layers is small compared to that of the core region, this yields:

$$r_{\text{diseng}} = \frac{G_{\text{down,bot}} - G_{\text{down,top}}}{\Delta z} \tag{2}$$

Note that the net disengagement rate represents the net balance between the rates of disengagement and reengagement. The value of r_{diseng} can be calculated for every position in the vertical direction based on the information on the solids concentration and solids velocity acquired through radar measurements, using Eq. (2).

The second solids back-mixing mechanism, i.e., the core-to-wall layer transfer of solids (represented by F_{lat} in Fig. 1), can be solved from the overall mass balance as:

$$F_{\text{lat}} = \left(\left(\text{G}_{\text{up,bot}}\text{-G}_{\text{down,bot}}\right)\text{-}\left(\text{G}_{\text{up,top}}\text{-G}_{\text{down,top}}\right)\right) A_{\text{z,core}} \tag{3}$$

This lateral transfer of solids from the core region to the wall layer can be described by means of a mass transfer coefficient for the core-to-wall layer solids back-mixing as:

$$\text{Flat} = \text{h}_{\text{m}} \text{A}_{\text{lat,core}} \;\; C_{\text{s}} = \text{h}_{\text{m}} (2(L_{\text{x,core}} + L_{\text{y,core}})\Delta z)\rho_s \varepsilon_{\text{s,core}} \tag{4}$$

Note that Eq. (4) expresses the core-to-wall solids transfer as a function of the solids concentration in the core and disregarding that in the wall layers. The reason behind this is the fact that this transfer mechanism has been shown to be not driven by a concentration difference (which indeed would yield a net transfer from the denser wall layers to the more disperse core region, contrary to experimental observations) but by turbophoresis [42], with the net transfer strongly dominated by the highly fluctuating solids flow in the core region depositing into the wall layers characterized by solids with very small velocity fluctuations.

Calculation of the values for the solids flux [Eqs. (1)–(3)], the disengagement volumetric rate [Eq. (2)], and the net core-to-wall layer mass transfer coefficient [Eq. (4)]), requires the vertical profiles of the solids concentration and distributions of the solids axial velocity in the core region, which can be obtained from the high-frequency radar technique [31,47], as detailed in the next section.

2.2. Radar diagnostics for solids fluxes

The present work employs radar-Doppler measurements along the height of the riser to derive the vertical profiles of the solids concentration (see Eq.5 below) and the vertical velocity distributions (by Doppler effect) of the solids. The particle concentration is calculated from the radar reflection signal, P_r, through Eq. (5) which takes into account the signal processing gains and losses [31]. The reflected radar signal, P_r, depends on the total solids cross section, i.e. in a combination of the particle concentration (through n_s) and particle size (through the particle cross section, σ_e). As a consequence, the reflected signal depends on the particle size distribution, f_{PSD}, as seen from the integrated function in the second exponential term in Eq. (5).

$$P_{\text{r}} = \frac{K}{R_{\text{R}}^4} n_{\text{s}} V_{\text{radar}} \int_{r=r_{\min}}^{r=r_{\max}} \text{f}_{\text{PSD}}(r)\, \sigma_{\text{b}}(r)\, \text{d}r \exp^{-2\int_{\text{l}=0}^{\text{l}=\text{R}} (\text{f}_{\text{ext}}\, n_{\text{s}}(\text{l}) \int_{\text{r}=r_{\min}}^{\text{r}=r_{\max}} \text{f}_{\text{PSD}}(\text{r})\, \sigma_{\text{e}}(\text{r})\, \text{d}r)\text{d}l} \tag{5}$$

Through Eq. (5) the particle number concentration, n_s (part/m^3), can be solved from the sampled reflected radar signal and later converted to the normalized solids volumetric concentration, ε_s, through Eq. (6):

$$\varepsilon_{\text{s}} = n_{\text{s}} V_{\text{part}} \tag{6}$$

Having the normalized solids volumetric concentration and mean velocity, the net solids flux can be calculated as:

$$G_{net} = \rho_{\text{s}} \varepsilon_{\text{s}} \overline{u}_s \tag{7}$$

Previous studies of the fluidized bed freeboard have assumed a fully

dispersed solids flow, so as to motivate setting the axial velocity of the solids to be equal to the difference between the gas velocity and the single particle terminal velocity, u_g-u_t [13,48]. However, owing to solids acceleration and non-fully dispersed conditions, the axial velocity of the solids varies with height, especially in the lower freeboard where solids entrainment by the gas flow and disengagement from the splash zone ballistic-like flow pattern occur [39]. This work disregards the assumption of perfectly dispersed solids flow, as radar measurements yield the distributions of the axial solids velocity along the height [46,47].

Given a solids suspension with a certain concentration, C_s, and distribution of axial velocities expressed as probability density function, $\beta(u_z)$, the upward and downward fluxes of solids can be calculated from integration of the solids velocity distribution.

$$G_{\text{down}} = C_s \int_{-\infty}^{0} \beta(u_z)\, u_z \mathrm{d}u_z \tag{8}$$

$$G_{\text{up}} = C_s \int_{0}^{\infty} \beta(u_z)\, u_z \mathrm{d}u_z \tag{9}$$

from which the net upwards flux of solids can be calculated as:

$$G_{\text{net}} = G_{\text{up}} - G_{\text{down}} \tag{10}$$

3. Experimental setup

Fig. 2 presents a schematic of the circulating fluidized bed unit used in this work, which is described in further detail elsewhere [49]. The unit is composed of acrylic glass and the riser has a cross-section of 0.5 × 0.9 m^2 and a height of 3.1 m. The circulating solids loop consists of a primary cyclone and a loop seal. The bed material used consists of glass beads with a density of 2,486 kg/m^3 and mean (Sauter, i.e. surface-based) particle diameter of 106 μm (d_{10} = 75 μm, d_{90} = 160 μm), i.e., Geldart B solids, yielding an average value of the single particle terminal velocity of 0.64 m/s. The unit is operated at room temperature and fluidized with air. Note that the experimental conditions in the present study do not apply any fluid-dynamic scaling, i.e., the solids flow established in the unit is only intended to represent qualitatively the solids flow in industrial, wide CFB risers. Although solids back-mixing by means of disengagement is expected to predominate along most of the riser, its significance should decrease with height, thereby allowing also observations of the solids back-mixing by means of lateral core-to-wall layers transfer.

The FMCW-pulse Doppler radar [50] utilized in this work operates at 0.34 THz (center frequency) and acquires the solids concentration and the distribution of axial solids velocity with a spatial resolution of 5 mm and a time resolution of 0.2 s. As shown in Fig. 3, the radar setup generates a horizontal radar beam, which by means of a metal mirror is redirected to penetrate the unit in the vertical direction from the riser roof (composed of high-density polyethylene to minimize signal attenuation) and extends itself along the vertical centerline of the riser. The radar beam penetrates the riser from the roof (see Fig. 3 [47]). In the measurement of both concentration and velocity, the accuracy depends mainly on the signal-to-noise ratio, which is strongly related to the central frequency and the particle sizes. Previous investigations with the same radar set-up in the same unit [31] revealed a good optimization of the central frequency and a mean difference to pressure-derived concentrations the measurement relative mean error is less lower than 25 %, with radar data showing clearly higher consistency and robustness, especially in the dilute regions..

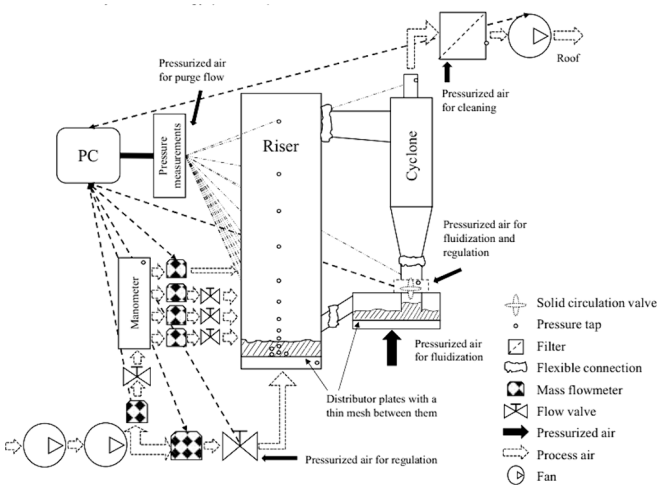

Fig. 2. Schematic of the circulating fluidized bed unit used in this work.

The riser pressure drop is kept constant at 1.3 kPa, while two superficial gas velocities (0.8 and 0.9 m/s, yielding u/u_t = 1.25–1.41) are applied to investigate the impacts of the gas velocity on the solids back-mixing mechanisms. These operational conditions optimized the performance of the radar measurement technique in terms of allowing penetration along the full height of the riser for the given bed material and radar frequency used – more details on the penetration ability of the radar signal can be found in [31]. The THz-radar measurement involves a sampling time of 1800 s over which data is time-averaged, ensuring statistical robustness.

4. Measurement procedure

The solids concentration values along the riser height are obtained from radar measurements according to Eqs. (5) and (6), yielding the profiles shown in Fig. 4. In Eq. (5) the Sauter mean size of the solids is used rather than the particle size distribution. This approach has been earlier been validated in previous studies with the same set-up: pressure drop measurements were carried out simultaneously to the radar sampling, revealing good agreement between both (see detailed analysis of several cases in [46]) and the better robustness of the radar technique at lower solid concentrations.

As shown, the solids concentration gradually decreases with height in the riser, with relatively strong decay along the freeboard regions immediately above the bottom region in CFB units operated with Geldart B solids, typically known as the 'splash zone' [42]. The exponential decay in solids concentration observed in previous experimental studies (for a compilation, see [39]) is for the current tests seen to be established at heights $h > 1$ m. At the top exit region (roughly $h > 2.5$ m), the solids concentration profile exhibits a strong decay related to effects from the riser exit.

Regarding the vertical solids velocity, Fig. 5 exemplifies the data acquired by the radar-Doppler with the example of a distribution measured at a height of 2.25 m for the 0.9 m/s case. Positive velocity values represent upwards solids flow, and vice versa. The markers in Fig. 5 show the measurement data acquired, while the solid line represents the fitted polynomial function used for later calculations [Eqs. (8) and (9)]. For data such as plotted in Fig.5, the fraction of the area below the curve located on the positive side of the x-axis indicates the share of particles flowing upwards (70.5 % in this case, meaning 29.5 % of the solids concentration at that location is flowing downwards). The solids flux upwards results from combining the velocity distribution data such as that in Fig.5 with the solids concentration (see Eq.9), which for the data in Fig.5 results in 1.22 kg/m^2s. Analogously, for the downflowing solids (Eq.8), a solids flux of 0.27 kg/m^2s is obtained. The net flow can be calculated as the difference between these two, or directly by expanding the integration limits to the whole x-axis. Note that data in Fig.5 indicate that occasionally solids with a vertical velocity as high as 2 m/s are detected. This is a consequence of the operation combining a low pressure drop gas distributor (to resemble those used in industrial CFB boilers, see details in [36]) and a pressure drop allowing the

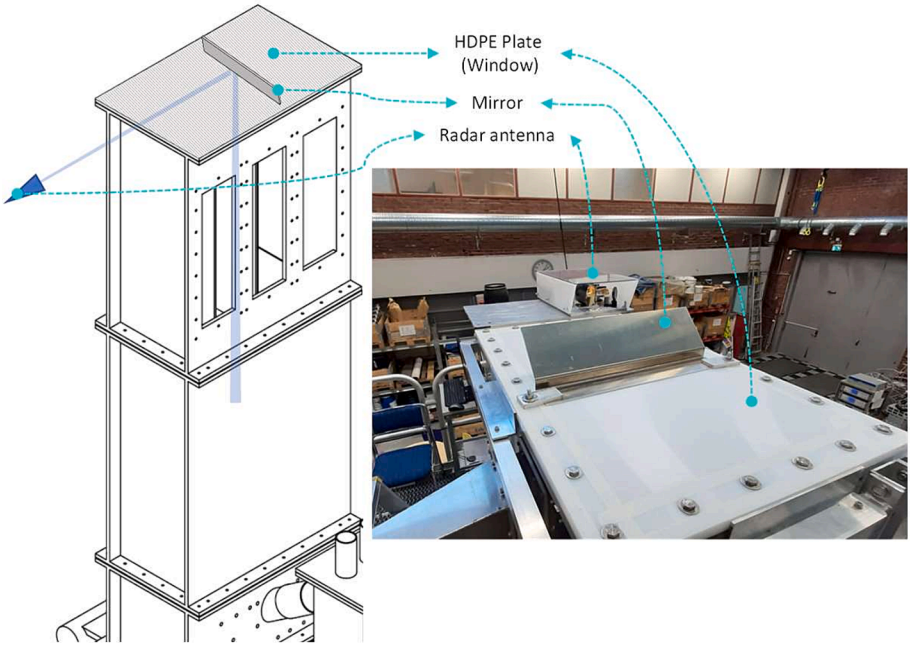

Fig. 3. Schematic of the experimental setup used for radar measurements [45].

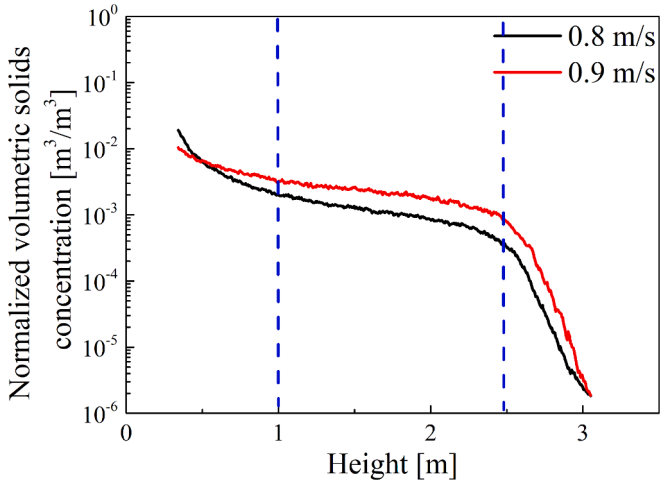

Fig. 4. Vertical profile of the radar-measured volumetric solids concentration in the core region. The region comprised between the blue dashed lines indicates the main zone of analysis, cropping out the bottom (splash) and exit regions. (For interpretation of the references to colour in this figure legend, the reader is referred to the web version of this article.)

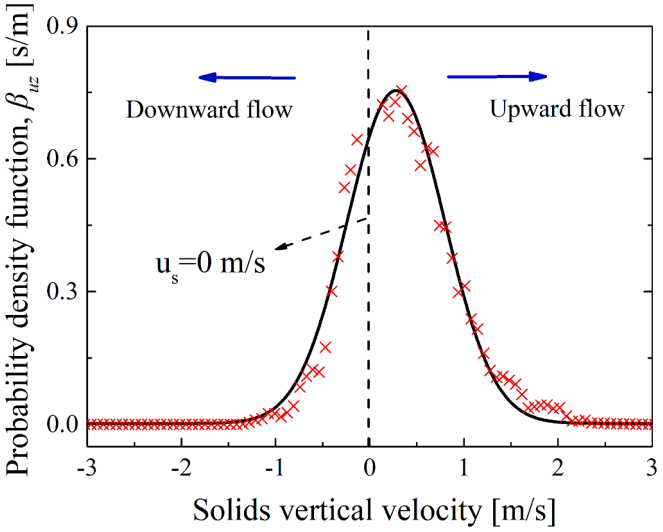

Fig. 5. Radar-measured probability density function of the vertical solids velocity at a height of 2.25 m (markers), together with the corresponding polynomial fitting (solid curve). u_g = 0.9 m/s.

presence of a dense bed, which yields strong pressure fluctuations in the air plenum, and thus instantaneously very high local gas velocities at the dense bed surface (Olowson and Almstedt [51] measured gas velocities up to 10 m/s for excess gas velocities of only 0.6 m/s) which persist to a minor extent at upper locations in the riser.

Fig. 6 shows the curves for the velocity distributions (and their corresponding mean values) at four different heights for a given gas superficial velocity. For these specific conditions, a height of 0.72 m falls within the splash region, in which strong ballistic-like solids backmixing yields a mean value of the solids axial velocity of close to 0 (albeit still positive, since there is a net solids upflow). As the height increases, the mean axial velocity also gradually increases, indicating that the solids upflow is more significant than the solids downflow. Note also the presence of particles with axial velocities higher than the gas velocity at all heights. As shown by Djerf et al. [49], even in cases where the low solids inventory yields the absence of a dense bed region, a splash zone is established with a relatively strong decay in solids concentration and both spatial and temporal fluctuations of the gas velocity. This fluctuating pattern with gas strokes and local high velocities even in absence of a dense bed with bubbles is believed to be originated by the use of a low pressure drop hole plate as gas distributor, yielding flow instabilities in the bottom region which are observed all along the height of the riser in the form of local temporary high velocity strokes (so-called *ghost bubbles* in literature, see [52]). Fig. 7 shows the axial upward particle velocity distribution in the riser for a gas superficial velocity of 0.9 m/s. The acceleration area is mainly distributed in the splash zone at the height of 0.5–1.0 m. Due to the influence of riser outlet, the particle velocity rapidly decreases above the height of 2.5 m. It is necessary to consider the acceleration and deceleration effects in the splash zone and riser outlet to correct the pressure-derived concentration values. While

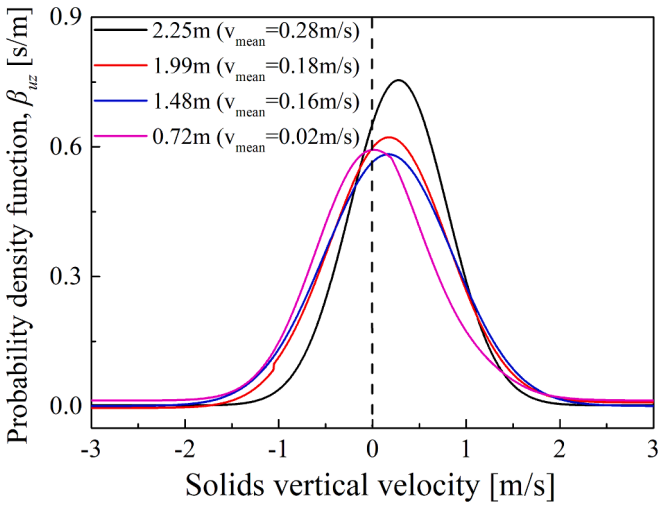

Fig. 6. Probability density functions of the vertical solids velocity, at different heights in the riser (u_g = 0.9 m/s).

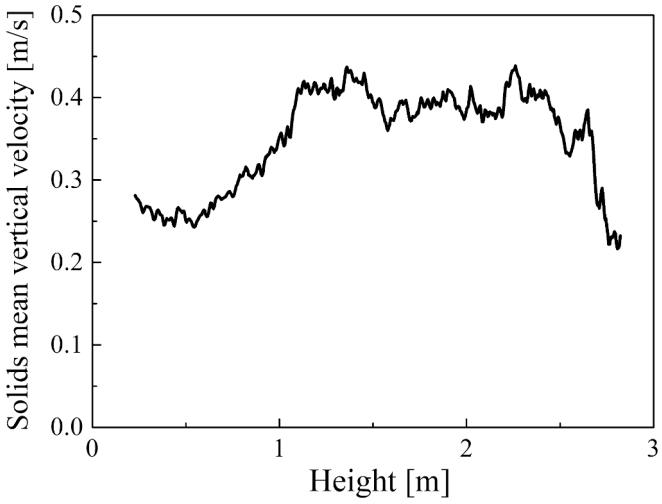

Fig. 7. Average vertical solids velocity along the riser (u_g = 0.9 m/s).

in the freeboard zone, the acceleration effect can be ignored.

5. Results and discussion

5.1. Axial solids flux

Fig. 8 shows the vertical profiles of the upward (dashed lines) and downward (solids lines) solids fluxes, calculated according to Eqs. (8) and (9), for different fluidization velocities. As seen from the solids flux profiles in Fig. 8, there is for both cases a significant presence of downflowing solids phase in the core region. The measurements were restricted to the height interval of 1.0–2.5 m (see Fig. 4), since the focus is on the region for which the flow is developed. As expected, both the upflow and downflow solids fluxes decrease with height, in similarity to the solids concentration. It is clear that an increase in fluidization velocity yields higher solids flux values at a given height in the riser. Fig. 9 shows the vertical profiles of solids flux in both axial directions as a function of the solids concentration. As seen, the gas velocity has little impact on the curves and in average the upwards solids flow at a higher absolute velocity than the downwards solids.

Fig. 10 shows the variation of the downward-to-upward flux ratio in the core region with height. This directional ratio is close to 1 at the

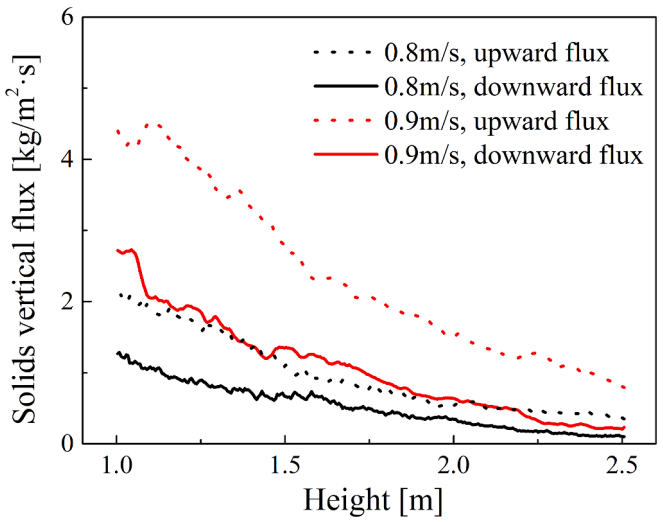

Fig. 8. Vertical profiles of the upward and downward solid fluxes, for two superficial gas velocities.

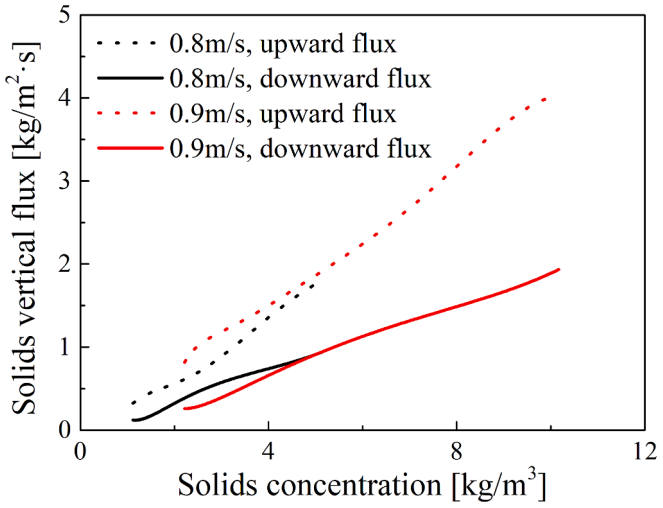

Fig. 9. Upward and downward solids flux as a function of the solids concentration, for two superficial gas velocities.

lower height levels, i.e., at the lower levels close to the splash zone, the radar measurements confirm that the solids flow is dominated by strong solids back-mixing due to solids splashes being ejected from the bottom region and following a ballistic flow pattern back downwards [39]. The downward-to-upward flux ratio decreases gradually along the riser height, to reach a value of 0.3 at the outlet height level. The superficial velocity has no significant impact on the ratio for the flow conditions in the unit used here. The data in Fig. 9 show that the downward-to-upward flux ratio remains at relatively high values in the freeboard (indicating dominance of the disengagement back-mixing). Industrial-scale measurements in tall ($h > 10$ m) risers [28,40] have shown that the downward-to-upward solids flux ratio approaches a relatively low value at height levels above those covered in this study, i.e., there is a low concentration of the downflowing phase in most of the transport zones of CFB boilers. Thus, it is important to note that the solids flow conditions established in the experimental setup used in this work (a wide, 3 m-tall riser with a shallow bed of Geldart group B solids) is expected to be representative only for the lower-most freeboards of CFB furnaces and not for the whole furnace height.

The net upward solids flux profiles [Eq. (10)] are presented in Fig. 11. The curves reveal a descending trend with height, which is due

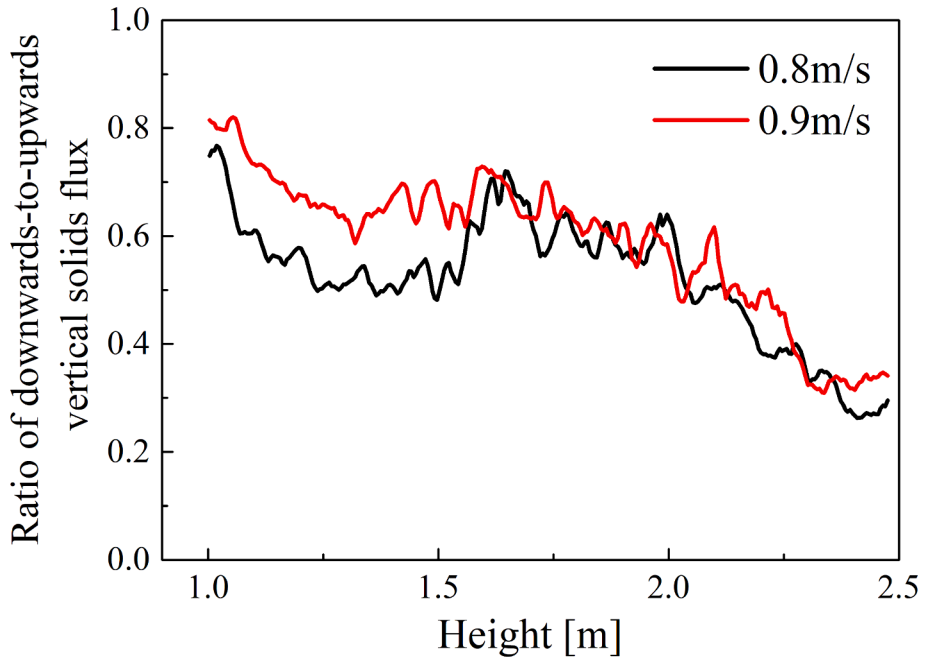

Fig. 10. Downward-to-upward axial solids flux ratio along height of the riser, for two superficial gas velocities.

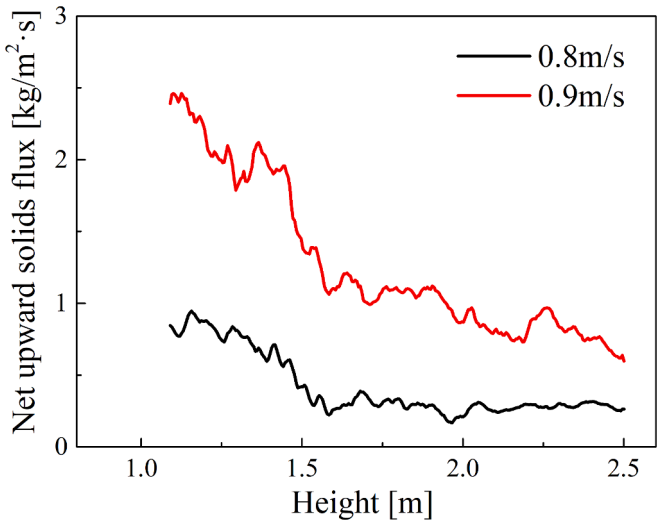

Fig. 11. Vertical profile of the net upward solids flux, for two superficial gas velocities.

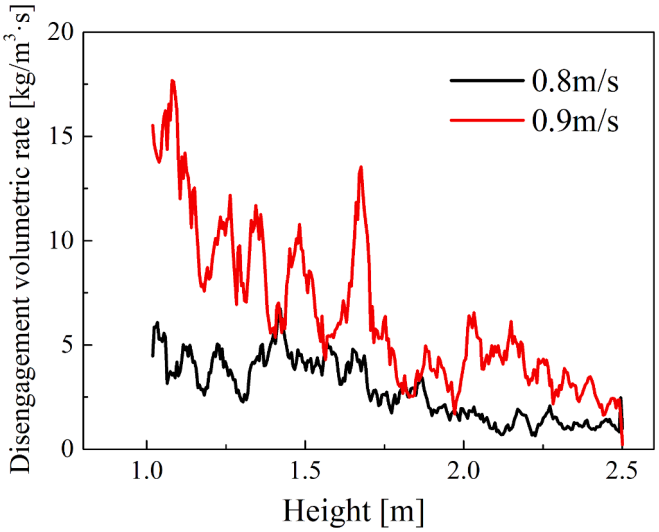

Fig. 12. Vertical profile of the net volumetric disengagement rate, for two superficial gas velocities.

to solids back-mixing to the wall layers (since solids back-mixing by disengagement alone would not yield a decrease in the net solids upflow in the core region). For any given height level, an increase in the gas velocity yields faster decay with height of the net solids flow, indicating increased solids transfer from the core region to the wall layers. Furthermore, at any given height, an increased gas velocity yields an increase in solids net upflow, as expected, and this is due to increased solids entrainment from the bottom region [49]. A noticeable decrease in the rate of net upward solids flux occurs at the height of 1.5 m, which is attributed to horizontal mass transfer.

5.2. Net disengagement rate

Fig. 12 shows the vertical profiles of the net volumetric disengagement rate, as obtained from the radar measurements [Eq. (2)]. The disengagement rate decreases gradually with height and increases with the gas superficial velocity at a given height. In order to gain further insights into the disengagement rate, Fig. 13 presents the measured disengagement rate as a function of the solids concentration, disclosing a coherent, strong and non-linear increase in disengagement rate with solids concentration. It must be noted that Fig. 13 includes data from the height range 0.3–2.5 m, i.e. extended towards the bottom region in comparison to the data shown in Fig. 12. This yields the inclusion in Fig. 13 of data points with much higher disengagement rate values. Higher solids concentrations have been reported in the literature as encouraging disengagement by cluster formation [53–55]. For the conditions investigated, as shown in Fig. 13, a higher gas velocity yields a higher disengagement rate for a given solids concentration. The data for the case with a gas velocity of 0.8 m/s (which covers the widest range of solids concentration) can be fitted as $r_{clust} = 1.22\, C_s^{2.45}$.

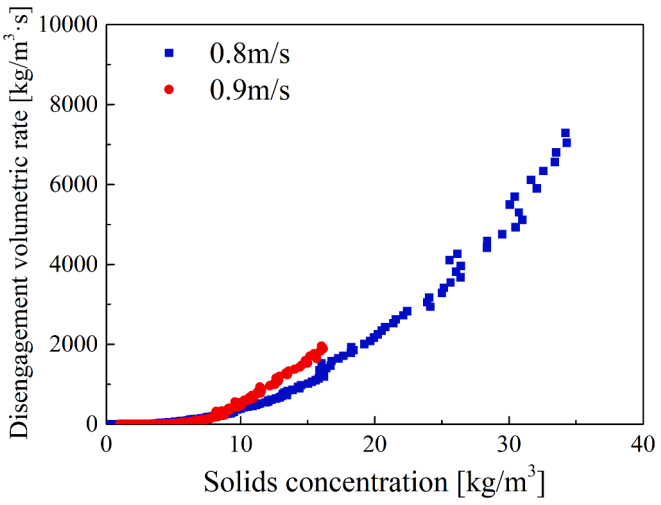

Fig. 13. Net volumetric disengagement rate as a function of the solids concentration, for two superficial gas velocities.

5.3. Solids transfer from the core region to wall layers

Fig. 14 illustrates the horizontal transfer of solids from the core region to the wall layer by showing the vertical profiles of the net transferred solids flux (based on lateral, i.e. core-layer, interfacing area). For the data processing related to Figs. 14 and 15, the experimental noise in the vertical profiles of solids velocity and concentration was removed by applying a 6th degree polynomial to the curves originally obtained. The lateral transfer rate of the solids decreases gradually with height, and at a given height increases with the gas superficial velocity, i.e., with increased local gas velocity and local solids concentration.

Fig. 15 shows the vertical profiles for the mass transfer coefficient governing the core-to-layer solids transfer [Eq. (4)]. The calculated values of this coefficient decrease with height and yield roughly stable values at $h > 1.8$ m, yielding 0.0038 and 0.0135 m/s, respectively, for the gas superficial velocities of 0.8 and 0.9 m/s. An increased fluidization velocity, which yields increases in the solids concentration and gas velocity at a given height, increases the mass transfer coefficient. This is in good agreement with an earlier study [42] that collected measurement data from a wide size range (12–460 MW) of CFB furnaces, and that showed an increase in the core-to-layer mass transfer coefficient with the gas velocity (and the riser cross-sectional dimensions). While that study used measurement data with poor vertical resolution (typical for commercial-scale units, with very few pressure taps above heights of tens of meters), the present work provides measurements with high spatial resolution (in the mm-scale) and reveals that, for the first meters above the gas distributor, there is a local decrease in the lateral mass transfer coefficient with height. It should be noted that this trend cannot be directly extrapolated to the upper heights, i.e., to most of the freeboard in large-scale CFB furnaces. Instead, it is to be regarded as an observation that is representative for the lower levels in the freeboards of large-scale units.

It should be noted that the calculated values of the mass transfer coefficient depend on the dimensions of the core region rather than those of the whole riser cross-section. The above values are calculated assuming a reference value for the wall layer thickness of 0.01 m at all height levels, based on the literature [8]. The sensitivity of the calculated mass transfer coefficient for the wall layer thickness is studied by considering also wall layer thicknesses of 0.005 m and 0.02 m, which fall within the typical range of observations [6]. The degree of sensitivity falls roughly within [-3.5, +1.8]%.

5.4. Comparison of the back-mixing mechanisms

The significance of each of the two solids back-mixing mechanisms was evaluated and exemplified by the case with the superficial velocity of 0.9 m/s, using Eqs. (1), (3) and (9) in Fig. 16. This revealed how the solids flow entrained from the bottom region (1.7 kg/s) is back-mixed by means of each mechanism along the height in the riser. At the lower height levels, solids are mainly back-mixed by means of disengagement, although the disengagement rate decreases relatively rapidly with height and eventually becomes lower than the horizontal mass transfer rate. In summary, for the case studied, about 10 % of the solids entrained from the bottom region reach the exit region, while around 50 % are

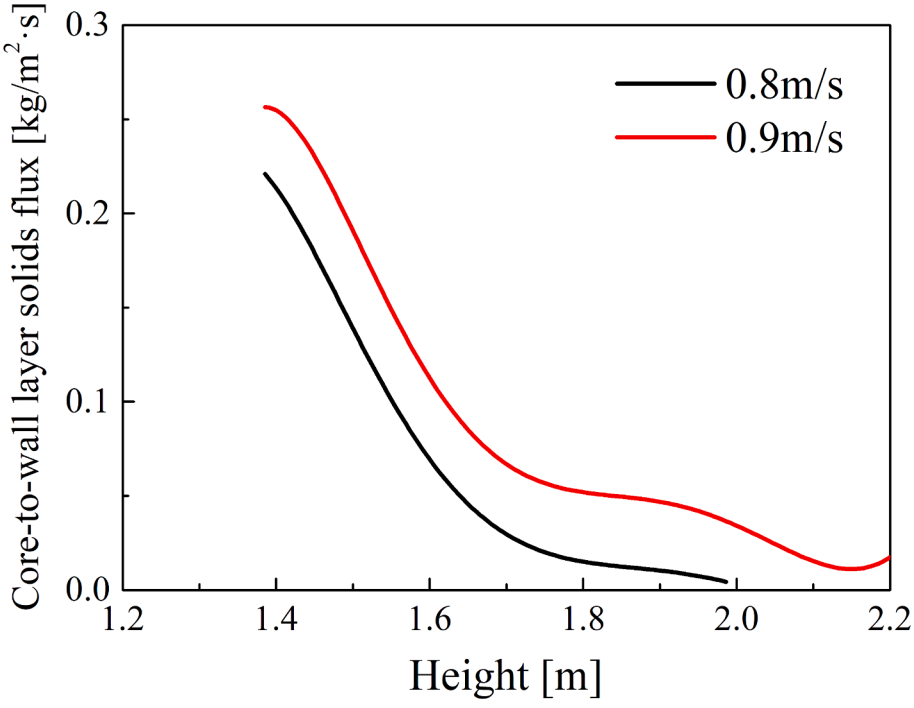

Fig. 14. Vertical profile of the net solids flux horizontally transferred from the core region to the wall layer, for two superficial gas velocities.

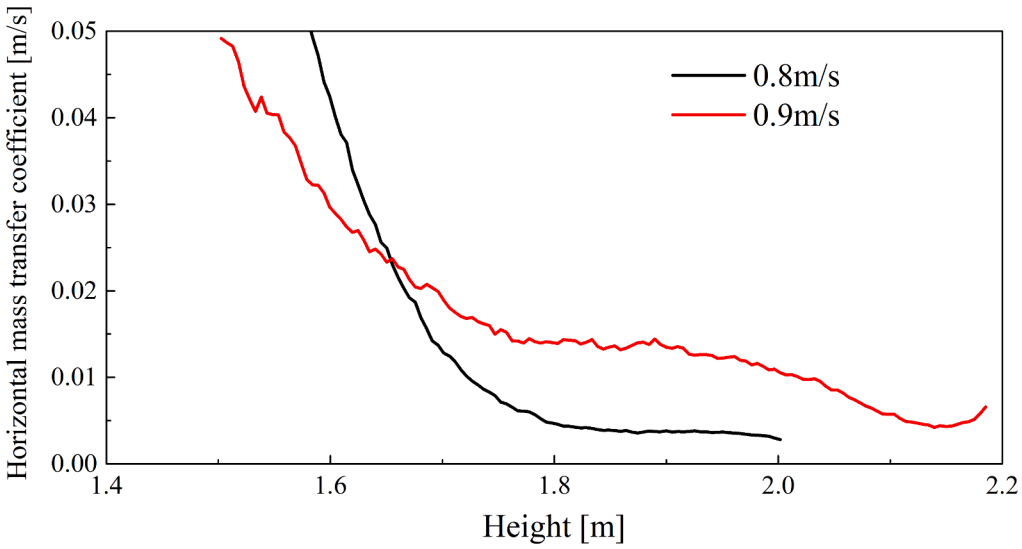

Fig. 15. Mass transfer coefficient for the core-to-layer solids transfer (Eq. 14), for two superficial gas velocities.

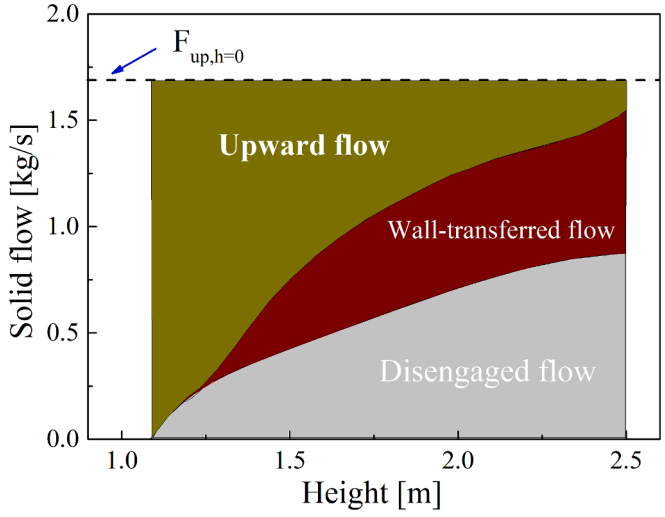

Fig. 16. Diagram of the axial solids backmixing flow along the height of the riser (u_0 = 0.9 m/s).

back-mixed by means of disengagement, and 39 % are back-mixed through transfer to the wall layers.

6. Conclusions

Solids back-mixing was investigated in the freeboard of a circulating fluidized bed operated under ambient conditions but with a geometry that is characteristic of large-scale CFB risers (3 m in height and a riser cross section of 0.4 × 0.4 m) and operated with Geldart B solids. The radar technique was applied to measure highly-resolved vertical profiles of the solids concentration and solids velocity distributions. The measurements provide closure of the mass balances across the height, thereby allowing determination of the vertical profiles of the net volumetric disengagement rate and the horizontal mass transfer coefficient. Two cases that differed with respect to superficial gas velocity were studied. Previous findings obtained through other experimental techniques, mainly pressure drop measurements, have been refined using the more accurate and resolved radar technique, which opens up the way for more-detailed future analyses of the riser flow dynamics – also in other applications. In terms of net contribution, the following major conclusions are drawn from the present study:

(1) The net volumetric disengagement rate increases with gas velocity and exhibits a strong non-linear growth with the solids concentration $\left(r_{diseng} \propto C_s^{2.45}\right)$;
(2) The core-to-wall layer mass transfer coefficient increases with the gas velocity, and exhibits an initial decay with height in the riser before fully developing into a stable level;
(3) For the set-up and operational conditions studied, the two solids back-mixing mechanisms are contributing roughly equally much. Extrapolation of this to CFB boiler furnaces is however not straight-forward, since the taller riser would weaken the relative significance of solids disengagement while the increased cross section-to-perimeter ratio would weaken that of the core-to-layers path for solids backmixing.

CRediT authorship contribution statement

Wanqiang Wu: Writing – original draft, Methodology, Investigation, Formal analysis, Data curation, Conceptualization. **Diana Carolina Guío-Pérez:** Data curation, Resources, Writing – original draft. **Marlene Bonmann:** Resources. **Filip Johnsson:** Supervision, Writing – original draft. **Lunbo Duan:** Supervision. **David Pallarès:** Writing – original draft, Validation, Conceptualization, Data curation, Formal analysis, Investigation, Methodology, Supervision.

Declaration of competing interest

The authors declare that they have no known competing financial interests or personal relationships that could have appeared to influence the work reported in this paper.

Data availability

Data will be made available on request.

References

[1] B. Leckner, L. Thorson, J. Kjärstad, F. Johnsson, Utilization of fluidized bed boilers —a worldwide overview, in Developments in Fluidized Bed Conversion 2011 to 2016. 2016, IEAFBC TCP: Presented at IEA-FBC 73rd Technical Meeting, Tokyo, Japan (December 2016).
[2] B. Leckner, Developments in fluidized bed conversion of solid fuels, Thermal Science 20 (2016) 1–18.

[3] A.V. Bridgwater, Review of fast pyrolysis of biomass and product upgrading, Biomass & Bioenergy. 38 (2012) 68–94.
[4] J.L.J. Ling, W. Yang, H.S. Park, H.E. Lee, S.H. Lee, A comparative review on advanced biomass oxygen fuel combustion technologies for carbon capture and storage, Energy. 284 (2023) 128566.
[5] G.M. Castilla, D.C. Guío-Pérez, S. Papadokonstantakis, F. Johnsson, D. Pallarès, Techno-economic assessment of calcium looping for thermochemical energy storage with CO2 capture, Energies. 14 (11) (2021) 3211.
[6] D. Pallarès, F. Johnsson, Macroscopic modelling of fluid dynamics in large-scale circulating fluidized beds, Prog. Energy Combust. Sci. 32 (2006) 539–569.
[7] D.N. Mondal, S. Kallio, H. Saxén, J. Hassel, Experimental study of cluster properties in a two-dimensional fluidized bed of Geldart B particles, Powder Technol. 291 (2016) 420–436.
[8] A. Johansson, F. Johnsson, B. Leckner, Solids back-mixing in CFB boilers, Chem. Eng. Sci. 62 (2007) 561–573.
[9] L. Hua, J. Wang, Residence time distribution of particles in circulating fluidized bed risers, Chem. Eng. Sci. 186 (2018) 168–190.
[10] J.C. Chen, Experiments that address phenomenological issues of fast fluidization, Chem. Eng. Sci. 54 (1999) 5529–5539.
[11] B. Deng, Y. Zhang, M. Zhang, H. Kong, T. Zhou, X. Yang, H. Yang, Identification and dynamic properties of clusters for Geldart group B particles in a circulating fluidized bed, Chem. Eng. Sci. 248 (2022) 117265.
[12] J.R.V. Ommen, J.V.D. Schaaf, J.C. Schouten, B.G.M. van Wachem, M.O. Coppens, C.M. van den Bleek, Optimal placement of probes for dynamic pressure measurements in large-scale fluidized beds, Powder Technol. 139 (2004) 264–276.
[13] T. Karlsson, X. Liu, D. Pallarès, F. Johnsson, Solids circulation in circulating fluidized beds with low riser aspect ratio and varying total solids inventory, Powder Technol. 316 (2017) 670–676.
[14] Y. Chen, Z. Tian, Z. Miao, Analysis of the pressure fluctuations in binary solids circulating fluidized bed, Energ. Convers. Manage. 47 (2006) 611–623.
[15] R. Feng, J. Li, L. Dong, Z. Hao, Z. Ba, H. Zhan, Y. Fang, Gas-solid flow behaviors in a multi-stage circulating fluidized bed under elevated pressure, Chem. Eng. Sci. 196 (2019) 1–13.
[16] P. Schlichthaerle, J. Werther, Axial pressure profiles and solids concentration distributions in the CFB bottom zone, Chem. Eng. Sci. 54 (1999) 5485–5493.
[17] J.R. van Ommen, S. Sasic, J. van der Schaaf, S. Gheorghiu, F. Johnsson, M. O. Coppens, Time-series analysis of pressure fluctuations in gas–solid fluidized beds - A review, International Journal of Multiphase Flow. 37 (2011) 403–428.
[18] J. Liu, J.R. Grace, X. Bi, Novel multifunctional optical-fiber probe: I, Development and Validation. Aiche J. 49 (2003) 1405–1420.
[19] H. Johnsson, F. Johnsson, Measurements of local solids volume-fraction in fluidized bed boilers, Powder Technol. 115 (2001) 13–26.
[20] M. Qi, J. Zhu, S. Barghi, Particle velocity and flux distribution in a high solids concentration circulating turbulent fluidized bed, Chem. Eng. Sci. 84 (2012) 437–448.
[21] X. Wei, J. Zhu, Tracking the flow dynamics in circulating fluidized bed through high-speed photography, Ind. Eng. Chem. Res. 58 (2019) 17540–17548.
[22] H. Chen, Y. Ding, S. Gu, C. Geng, W. Sheng, Experiential investigation of cluster velocity and slip velocity in the CFB riser, Powder Technol. 370 (2020) 1–8.
[23] J. Xu, X. Lu, Q. Wang, W. Zhang, C. Liu, X. Xie, S. Sun, X. Fan, J. Li, Visualization of gas-solid flow characteristics at the wall of a 60-meter-high transparent CFB riser, Powder Technol. 336 (2018) 180–190.
[24] J. Ma, V. Ommen, J. Ruud, D. Liu, M. Robert, X. Chen, W. Evert, L. Cai, Fluidization dynamics of cohesive Geldart B particles. Part I: X-ray tomography analysis, Chem. Eng. J. 359 (2019) 1024–1034.
[25] C. Rautenbach, R.F. Mudde, X. Yang, M.C. Melaaen, B.M. Halvorsen, A comparative study between electrical capacitance tomography and time-resolved X-ray tomography, Flow Meas. Instrum. 30 (2013) 34–44.
[26] Q. Tu, H. Wang, Effects of riser geometry on gas–solid flow characteristics in circulating fluidized beds, Particuology. 49 (2020) 205–217.
[27] G. Qiu, J. Ye, H. Wang, W. Yang, Investigation of flow hydrodynamics and regime transition in a gas–solids fluidized bed with different riser diameters, Chem. Eng. Sci. 116 (2014) 195–207.
[28] A. Johansson, F. Johnsson, B. Leckner, E.U. Hartge, J. Werther, R. Sekret, A. Hotta, Solids flow pattern in circulating fluidized-bed boilers, VGB PowerTech 84 (2004) 82–92.
[29] H. Johnsson, F. Johnsson, Measurements of local solids volume-fraction in fluidized bed boilers, Powder Technol.. 115 (2001) 13–26.
[30] M.V. de Velden, J. Baeyens, K. Smolders, Solids mixing in the riser of a circulating fluidized bed, Chem. Eng. Sci. 62 (2007) 2139–2153.
[31] M. Bonmann, D.C. Guío-Pérez, T. Bryllert, D. Pallarès, M. Seemann, F. Johnsson, J. Stake, Sub-millimetre wave range-Doppler radar as a diagnostic tool for gas-solids systems - solids concentration measurements, Adv. Powder Technol. 34 (2023) 103894.
[32] A. Teplyuk, R. Knochel, G. Khlopov. Aerosol Particle Sensor based on “Millimeter Wave Coherent Radar with High Spatial Resolution” IMS 2009, Boston, USA, June 2009.
[33] A. Reinhardt, A. Teplyuk, R. Knöchel, M. Höft. Remote measurement of particle streams with a multistatic dual frequency millimeter wave radar sensor. 2018 IEEE/MTT-S International Microwave Symposium – IMS. 2018, 127-130.
[34] A. Reinhardt, A. Teplyuk, R. Knöchel, M. Höft, Size determination in particle streams using a multistatic dual frequency millimeter wave radar, 15th European Radar Conference. (2018) 413–416.
[35] F. Johnsson, W. Zhang, B. Leckner. Characteristics of the formation of particle wall-layers in CFB boilers. In: Proceedings of the Second International Conference on Multiphase Flow. 1995: 25-32.
[36] T. Djerf, D. Pallarès, F. Johnsson, Solids flow patterns in large-scale circulating fluidised bed boilers: experimental evaluation under fluid-dynamically down-scaled conditions, Chem. Eng. Sci. 231 (2021) 116309.
[37] C. Baer, T. Jaeschke, P. Mertmann, N. Pohl, T. Musch, A mm-wave measuring procedure for mass flow monitoring of pneumatic conveyed bulk materials, IEEE Sensors Journal. 14 (2014) 3201–3209.
[38] T. Bryllert, M. Bonmann, J. Stake. A Submillimeter-Wave FMCW Pulse-Doppler Radar to Characterize the Dynamics of Particle Clouds. IEEE Transactions on Terahertz Science and Technology. 2301.00558.
[39] T. Djerf, D. Pallarès, F. Johnsson, Solids backmixing and entrainment in the splash zone of large-scale fluidized bed boilers, Powder Technol. 404 (2022) 117471.
[40] B. Leckner, M.R. Golriz, W. Zhang, B.A. Andersson, F. Johnsson, Boundary layers - first measurements in the 12 MW CFB research plant at Chalmers University, in: 11th International Conference on Fluidized Bed Combustion, 1991, pp. 771–776.
[41] J.F. Davidson, Circulating fluidised bed hydrodynamics, Powder Technol. 113 (2000) 249–260.
[42] T. Djerf, D. Pallarès, F. Johnsson, G. Sardina, H. Ström, Solids back-mixing in the transport zone of circulating fluidized bed boilers, Chem. Eng. J. 428 (2022) 130976.
[43] W. Zhang, F. Johnsson, B. Leckner, Fluid-dynamic boundary layers in CFB boilers, Chem. Eng. Sci. 50 (1995) 201–210.
[44] A. Nikolopoulos, C. Samlis, M. Zeneli, N. Nikolopoulos, S. Karellas, P. Grammelis, Introducing an artificial neural network energy minimization multi-scale drag scheme for fluidized particles, Chem. Eng. Sci. 229 (2021) 116013.
[45] J. Werther, Fluid Mechanics of large-scale CFB units, Circul Fluid Bed Technol. (1993) 1–14.
[46] D.C. Guío-Pérez, M. Bonmann, T. Bryllert, M. Seemann, J. Stake, F. Johnsson, D. Pallarès, Radar-based measurements of the solids flow in a circulating fluidized bed, Fuel 345 (2023) 128232.
[47] D.C. Guío-Pérez, M. Bonmann, D. Pallarès, T. Bryllert, F. Johnsson. Radar-based measurements of the solids flow in a circulating fluidized bed-first experiences. Fluidization Bed Conversion Conference 2022, Göteborg, Sweden, May 2022.
[48] X. Mo, P. Wang, H. Yang, J. Lv, M. Zhang, Q. Liu, A hydrodynamic model for circulating fluidized beds with low riser and tall riser, Powder Technol. 274 (2015) 146–153.
[49] T. Djerf, D. Pallarès, F. Johnsson, Bottom-bed fluid dynamics-Influence on solids entrainment, Fuel Processing Technol. 173 (2018) 112–118.
[50] T. Bryllert, M. Bonmann, J. Stake. 340 GHz FMCW pulse-doppler radar, preprint available at https://research.chalmers.se /publication/530791 (June, 2022).
[51] P.A. Olowson, A.E. Almstedt, Influence of pressure and fluidization velocity on the bubble behaviour and gas flow distribution in a fluidized bed, Chem. Eng. Sci. 45 (1990) 1733–1741.
[52] S. Pemberton, J. Davidson, Turbulence in the freeboard of a gas-fluidised bed: The significance of ghost bubbles, Chem. Eng. Sci. 39 (1984) 829–840.
[53] T.Y. Yang, L.P. Leu, Multiresolution analysis on identification and dynamics of clusters in a circulating fluidized bed, AIChE J. 55 (2009) 612–629.
[54] M.H. Zhang, K.W. Chu, F. Wei, A.B. Yu, A CFD-DEM study of the cluster behavior in riser and downer reactors, Powder Technol. 184 (2008) 151–165.
[55] J.S. Yang, J. Zhu, A novel method based on image processing to visualize clusters in a rectangular circulating fluidized bed riser, Powder Technol. 254 (2014) 407–415.